Title

Zirconium isotopic composition of the upper continental crust through time

Authors

Tian, Shengyu
Moynier, Frederic
Inglis, Edward C
et al.

Publication Date

2021-10-01

DOI

10.1016/j.epsl.2021.117086

Peer reviewed

Zirconium isotopic composition of the upper continental crust through time

Shengyu Tian[a*], Frederic Moynier[a], Edward C. Inglis[a], Roberta L. Rudnick[b], Fang Huang[c], Catherine Chauvel[a], John B. Creech[d], Richard M. Gaschnig[e], Zaicong Wang[f], Jing-Liang Guo[f]

[a] *Université de Paris, Institut de Physique du Globe de Paris, CNRS, Paris cedex 05, France*

[b] *Department of Earth Science, University of California-Santa Barbara, Santa Barbara, California 93106, USA*

[c] *CAS Key Laboratory of Crust-Mantle Materials and Environments, School of Earth and Space Sciences, University of Science and Technology of China, Hefei 230026, China*

[d] *Department of Earth and Planetary Sciences, Macquarie University, NSW 2109, Australia*

[e] *University of Massachusetts – Lowell, Department of Environmental, Earth, and Atmospheric Science, Lowell, MA 01854, USA.*

[f] *State Key Laboratory of Geological Processes and Mineral Resources, School of Earth Sciences, China University of Geosciences, Wuhan 430074, China*

Abstract

The stable isotopic composition of insoluble, refractory elements such as titanium (Ti) or zirconium (Zr), which are modified by magmatic differentiation but, *a priori,* are poorly affected by weathering or diagenesis, serve as powerful potential proxies to reconstruct the compositional evolution of the continental crust. Here we present the evolution of the Zr stable isotopic compositions ($\delta^{94/90}Zr_{IPGP\text{-}Zr}$, per mille

deviation of $^{94}Zr/^{90}Zr$ from IPGP-Zr standard) of the continental crust trough time, using 38 sedimentary samples from the upper continental crust (UCC), including 12 Holocene loess from the Chinese Loess Plateau and Xinjiang, three oceanic sediments from the sea floor outboard of the Lesser Antilles island arc and 23 glacial diamictite composites with depositional ages ranging from ~ 2.9 Ga to 0.3 Ga from South Africa, South America, Canada, USA and China. The samples show limited Zr isotopic variations with $\delta^{94/90}Zr_{IPGP\text{-}Zr}$ values of 0.043‰ - 0.109‰ for loess; 0.069‰ - 0.083‰ for oceanic sediments and 0.031‰ - 0.118‰ for glacial diamictites; their Zr-weighted average values are, 0.081± 0.044‰ (2SD, n = 12), 0.073 ± 0.015‰ (2SD, n = 3) and 0.078 ± 0.047‰ (2SD, n = 23), respectively. The isotopic similarity among loess, oceanic sediments and glacial diamictites, suggests that zircon enrichment effects previously documented in some sedimentary samples have not biased the Zr isotope compositions of these sedimentary rocks from their source rocks. Two groups with or without Zr enrichment have similar average $\delta^{94/90}Zr_{IPGP\text{-}Zr}$ values (0.075 ± 0.040‰ and 0.080 ± 0.046‰). There is no correlation between Zr isotope compositions and any proxy of chemical weathering (e.g., Al_2O_3/SiO_2, Fe_2O_3/SiO_2, CIA, K_2O/Al_2O_3 and δ^7Li). The $\delta^{94/90}Zr_{IPGP\text{-}Zr}$ values are quite constant for these sedimentary samples regardless of their depositional ages and locations. Therefore, the UCC appears to have had a constant Zr isotopic composition between 3 Ga and present, and is homogeneous at a large scale. Combining data for sedimentary reference materials from the literature and the sedimentary rocks in this study, we

suggest a Zr-weighted $\delta^{94/90}Zr_{IPGP\text{-}Zr}$ value of 0.077 ± 0.058‰ (2SD, n = 44) for the UCC, which is statistically distinct (t test, p value = 2.88×10^{-10}) and higher than that of the mantle (0.040 ± 0.044‰, n = 72). Combining the $\delta^{94/90}Zr_{IPGP\text{-}Zr}$ values of different terrestrial reservoirs, the $\delta^{94/90}Zr_{IPGP\text{-}Zr}$ of the BSE and bulk Earth is constrained to be 0.041 ± 0.041‰.

Key words: zirconium isotopes, upper continental crust, BSE, glacial diamictites, loess, oceanic sediments

Introduction

The Earth is the only terrestrial planet with plate tectonics, though the timing of its initiation is still vigorously debated (Brown et al., 2020; Harrison, 2009; Korenaga, 2013). The production of the first felsic continental crust is usually taken as a proxy to trace the initiation of subduction and, by extension, plate tectonics (Greber et al., 2017; Tang et al., 2016). In particular, the concentrations of insoluble elements and their ratios in terrigenous sedimentary rocks have been used to deduce the bulk composition of the UCC over Earth history (Condie, 1993; Taylor and McLennan, 1985). Recently, based on the correlation between the stable Ti isotopic composition of igneous rocks with their SiO_2 content, Ti isotope ratios in Archean shales have been interpreted to reflect the presence of intermediate to felsic crust as early as 3.5 Ga (Greber et al., 2017). However, later work demonstrated that tholeiitic and calc-alkaline differentiation series produce different degrees of Ti isotope fractionation,

which could be interpreted as either a changing or constant UCC composition, depending on which types of igneous rocks dominated at a particular time (Deng et al., 2019; Hoare et al., 2020). Although not fully conclusive, the study of Ti isotope composition of sediments highlights the strong potential of using novel stable isotope tracers to shed new light on crustal evolution.

Zirconium isotopes have the potential to further trace magmatic differentiation and provide constraints on the formation and evolution of the continental crust (Guo et al., 2020; Ibañez-Mejia and Tissot, 2019; Inglis et al., 2019). Zirconium, like Ti, is a refractory (50% condensation temperature = 1741K; Lodders, 2003), incompatible, and insoluble element. Ratios of similarly insoluble, incompatible, high field-strength elements (HFSE) have been used to constrain mantle end members of intraplate magmas, provide information on the genesis and eruptive environments of lavas, and trace recycled crustal components in the mantle (Condie, 2005; Niu, 2004). Moreover, zircon, the main host of Zr in most crustal rocks, is critical in studies of the temporal evolution of both the crust and lithospheric mantle, due to its use for U-Th-Pb geochronology, Lu-Hf, and O isotope measurements (Dhuime et al., 2012; Harrison et al., 2005; Valley et al., 2005; Wilde et al., 2001).

Zirconium has five stable isotopes: ^{90}Zr (51.45%), ^{91}Zr (11.22%), ^{92}Zr (17.15%), ^{94}Zr (17.38%) and ^{96}Zr (2.8%), and fractionation of these isotopes is recorded using delta notation ($\delta^{94/90}Zr_{IPGP\text{-}Zr}$). A strong covariation is observed between Zr contents and Zr isotope compositions for lavas from the Hekla volcano, Iceland (Inglis et al.,

2019). For rocks with SiO_2 contents > ~66.8 wt.%, $\delta^{94/90}Zr_{IPGP\text{-}Zr}$ increases significantly, together with a sharp decrease of the Zr concentrations. This is likely caused by zircon fractionation from the residual melt (Inglis et al., 2019), creating an overall range of $\delta^{94/90}Zr_{IPGP\text{-}Zr}$ of 0.582‰. Moreover, *in situ* Zr isotopic studies within internally zoned zircons from the Gangdese arc, Tibet showed lighter isotope compositions in the cores and heavier values toward the rims, with an overall range of 1.27 ‰ (Guo et al., 2020). This study demonstrated that lighter Zr isotopes are preferentially incorporated into zircons, causing the residual melt to have heavier Zr isotope composition. On the other hand, zircon and baddeleyite crystals from the anorthositic gabbro GC-1 from the Duluth Complex were found to be enriched in the heavier Zr isotopes (Ibañez-Mejia and Tissot, 2019; Zhang et al., 2019), with an overall range of ~5 ‰. Recent *ab-initio* calculations suggested that while $\delta^{94/90}Zr_{IPGP\text{-}Zr}$ of zircon, in which Zr is in 8-fold coordination, should be lower than that of the silicate melt, in which Zr is in 6-fold coordination, equilibrium fractionation is too small to explain the fractionation observed in the Hekla, Duluth Complex, and Gangdese igneous systems, and that part of the light isotope enrichment of zircons is due to kinetic isotopic fractionation driven by diffusion (Chen et al., 2020; Méheut et al., 2020). Whatever the mechanism driving these isotopic fractionations, the large Zr isotopic variations due to magmatic differentiation suggest that Zr stable isotopes could be used as a new proxy to constrain the chemical compositional evolution of

105 UCC. A first step in that direction is to evaluate the Zr isotope composition of UCC
106 over time.

107 Studies of the average composition of the UCC traditionally follow one of two
108 approaches: establishing weighted averages of the compositions of outcrops at the
109 surface via large-scale sampling, or weighted averaging of fine-grained clastic
110 sedimentary rocks (e.g., shale, loess and glacial diamictites) (Condie, 1993; Rudnick
111 and Gao, 2014; Taylor and McLennan, 1985). The former approach is the primary
112 source of estimates of the average abundance of major elements and a number of
113 soluble trace elements in the UCC. The latter approach is used to derive the average
114 composition of insoluble elements in the UCC, assuming that sedimentation processes
115 provide a natural sampling of large areas of the exposed crust and elements with low
116 solubility are not impacted by weathering. Furthermore, this approach could also be
117 used to investigate the secular evolution of the UCC by utilizing sedimentary rocks of
118 various depositional ages. In addition to the two methods noted above, Plank and
119 Langmuir (1998) generated a global subducting sediment (GLOSS) composition and
120 flux based on average global oceanic sediments, in order to assess the influence of
121 subducting sediments on arc volcanism and crust-mantle recycling, and re-evaluate
122 the chemical composition of the continental crust. They found that the HFSE
123 abundances are closely related to the presence of detrital phases and GLOSS is
124 dominated by terrigenous materials (76 wt.%). (Plank and Langmuir, 1998).

Here we estimate the Zr isotopic composition of the UCC based on analyses of a variety of sedimentary samples: twelve Holocene loess deposits, three oceanic sediments and twenty-three glacial diamictite composites having depositional ages spanning much of Earth history (~2.9 - 0.3 Ga). As Zr is an insoluble element, its concentration and isotopic composition is not expected to be affected by chemical weathering. Loess experiences limited chemical weathering during formation but may have been affected by mineral sorting during transportation, such as zircon enrichment (e.g., Taylor et al., 1983). The loess studied here are from Yimaguan, Luochuan, and Nileke in China and have been previously well characterized (Gong et al., 2017; Hao et al., 2012; Nan et al., 2018; Tsai et al., 2014). The oceanic sediments have previously been characterized by Carpentier et al. (2008 and 2009). Their composition is mainly controlled by detrital materials from the continental crust (Carpentier et al., 2008). The glacial diamictite composites have been widely used to study the chemical compositions of UCC (Chen et al., 2016; Gaschnig et al., 2014; Gaschnig et al., 2016; Greaney et al., 2020; Johnson and Goldblatt, 2017; Li et al., 2016; Mundl et al., 2018; Nan et al., 2018; Wang et al., 2019). By studying the Zr isotope compositions of terrigenous sedimentary rocks we aim to constrain the Zr isotope composition of the UCC, its secular evolution between 3 Ga and present, and estimate whether mineralogical sorting and chemical weathering influences Zr isotope compositions of terrigenous sediments.

Methods and Samples

Loess

Loess is fine, silt-sized aeolian sediment derived from glacial outwash plains or from desert environments (Taylor et al., 1983). Pleistocene loess covers 10% of Earth's surface (Taylor et al., 1983). Loess exhibits CIA values (CIA = molar proportions $Al_2O_3 / (Al_2O_3 + K_2O + Na_2O + CaO^*)$, where CaO* is CaO amounts contributed by silicate fraction of the whole sample) slightly above that of fresh igneous rocks, and lower than typical CIA values of shales. The chemical weathering signal in loess may also originate from glacially eroded bedrocks (Gallet et al., 1998). Loess samples from around the world have similar rare earth element patterns, akin to those seen in post-Archean shales (Taylor et al., 1983). As aeolian processing does not seem to fractionate most incompatible and insoluble elements from lanthanum except those affected by heavy mineral fractionation, loess is taken to provide a robust estimate of the abundance of these elements in the UCC based on their ratios with lanthanum (Taylor et al., 1983).

Eleven loess and one paleosol samples were collected from Yimaguan, Luochuan, and Nileke, China (Table S1). The Yimaguan and Luochuan loess-paleosol sections are representative of the Chinese Loess Plateau and was deposited over the past 0.9 Ma. These samples comprise wind-rafted sediments from inland deserts in northern and northwestern China and were previously used to determine the timing of build-up of the northern hemisphere ice sheets (Hao et al., 2012) and to estimate the Fe and Ba isotope compositions of the UCC (Gong et al., 2017; Nan et al., 2018).

Xinjiang is one of the most significant loess regions in China and Central Asia, and is situated between the East Europe loess region and the well-studied Chinese Loess Plateau. Xingjiang loess is mainly derived from adjacent deserts, transported via northwesterly winds (Tsai et al., 2014). The Xinjiang loess samples in this study have also been used to constrain the Ba isotopic composition of the UCC (Nan et al., 2018).

Oceanic sediments

Oceanic sediments are primarily composed of products of erosion of the continental crust, and biologically and chemically precipitated minerals (Carpentier et al., 2009; Plank and Langmuir, 1998). The final composition of the sediments depends on the distance to the detrital sources, biological productivity, carbonate compensation depth and sedimentation rate (Carpentier et al., 2009). Plank and Langmuir (1998) established the composition of global subducting sediment (GLOSS) and found that GLOSS is dominated by terrigenous materials (76 wt.% terrigenous, 7 wt.% calcium carbonate, 10 wt.% opal, 7 wt.% mineral-bound H_2O^+). Therefore, GLOSS is similar to the UCC in composition (Plank and Langmuir, 1998).

Three oceanic sediment samples, which were collected from DSDP 14 Site 144 (at 2960 m water depth) on the Demerara Rise, and DSDP 78A Site 543 (at 5630 m water depth), located to the east of Dominica Island, were analyzed for their Zr isotope composition. Site 144 is situated southeast of the Lesser Antilles island arc, closer to the South American continent (340 km) compared to Site 543 (860 km)

188 (Carpentier et al., 2008; Carpentier et al., 2009). Some Site 144 sediments exhibit
189 remarkable Zr and Hf enrichments, which are attributed to enrichment of zircons in
190 coarse detrital fractions (Carpentier et al., 2009), including the two samples selected
191 for this study. By contrast, the sediments from site DSDP 543 are enriched in finer
192 clay-rich fractions devoid of zircon (Carpentier et al., 2009). These samples have been
193 well characterized for trace elements and Sr-Nd-Pb-Hf, Li and Mo isotope
194 compositions (Carpentier et al., 2008; Carpentier et al., 2009; Gaschnig et al., 2017;
195 Tang et al., 2014). Overall, the sediments from Site 144 and 543 are dominated by
196 input from old detrital continental materials that have different compositions. For the
197 samples studied here, the two from site 144 show the effects of detrital quartz and
198 zircon enrichment, while the one from site 543 is dominated by detrital clays. The
199 CIA values of the three samples vary from 61 to 66, which is slightly higher than
200 those of the loess samples in this study (from 57 to 64 with an average of 60).

201 **Glacial diamictites**

202 Goldschmidt (1933) first noted that glacial loam may provide a means of
203 determining the average composition of the UCC. Nevertheless, it took nearly 80
204 years for geoscientists to begin to explore these deposits for this purpose (Gaschnig et
205 al., 2014). Glaciers mechanically erode the soil and bedrock that they traverse,
206 producing comminuted sediments that approximate the average of the soils and rocks
207 underlying the glaciers. When the glaciers melt, their sedimentary load is deposited as
208 glacial till, which is later lithified. These deposits may occur on land or in the shallow

209 marine environment (Gaschnig et al., 2014). Minimal chemical weathering is
210 expected to have occurred during erosion, transport and deposition due to the low
211 temperatures and the rapid deposition of the diamctites. Compared to loess and shales,
212 glacial diamictites are not reworked by wind or water (Gaschnig et al., 2014; Rudnick
213 and Gao, 2014; Taylor and McLennan, 1985). Twenty-three glacial diamictite
214 composites comprised of more than 100 individual samples with depositional ages
215 ranging from 2.9 Ga to 0.3 Ga from South Africa, South America, Canada, USA and
216 China, were analyzed for their Zr isotopic composition (Table S2). The glacial
217 diamictites have been previously well characterized for their chemical compositions
218 (Chen et al., 2016; Gaschnig et al., 2014; Gaschnig et al., 2016), and a wide range of
219 isotopic compositions (Li, N, O, Mo, Nd, Hf-W, Ba, and Ni; Gaschnig et al., 2016;
220 Greaney et al., 2020; Johnson and Goldblatt, 2017; Li et al., 2016; Mundl et al., 2018;
221 Nan et al., 2018; Wang et al., 2019). Most of the composites have elevated CIA
222 values relative to the values of fresh igneous rocks (Nesbitt and Young, 1982) and are
223 depleted in Sr, reflecting the influence of chemical weathering. Li et al. (2016) used
224 lithium isotopes and Pb isotopes, along with chemical, petrographic, and outcrop data
225 to evaluate the origin of this weathered signature. They concluded that the signatures
226 are mainly inherited from the UCC traversed by the glaciers rather than during syn- or
227 post- depositional weathering.

228 **Other samples**

In addition to the terrigenous sedimentary rocks described above, we evaluate Zr isotopic data of sedimentary reference materials including shales, river, or lake sediments to derive an estimate of the Zr isotope composition of the UCC and the BSE. They are: stream sediments JSD-1and JSD-2, lake sediments JLK-1, and shales SCo-1, SBC-1 and SGR-1 (Table S3).

Analytical methods

The loess and oceanic sediment samples (Carpentier et al., 2008) were hand crushed to powders in an agate mortar. The preparation of the glacial diamictite composites was described in detail in Gaschnig et al. (2016). The powders were digested using 2 mL mixture of 27 M HF and 16 M HNO_3 at a 5:1 ratio within PTFE vials. These vials were placed within spring-loaded screw-top steel vessels obtained from Parr Instruments® (typically referred to as Parr bombs). After heating at 160 ℃ for five days the sample solutions were evaporated to dryness and treated with 2 mL 6M HCl on a hot plate at 140 ℃ for two days for fluoride decomposition.

An aliquot containing ~1 μg Zr obtained from each solution was dried down, brought back into solution in 2 mL of 4 M HF and spiked with a ^{91}Zr-^{96}Zr double-spike (51.4% ^{91}Zr and 48.6% ^{96}Zr) at an optimal spike to sample ratio of 43:57. Before chemical separation, the spiked solutions were heated at 120 ℃ for at least 12 hours to equilibrate the samples and double spike. Zirconium separation was achieved using a procedure described in Tian et al. (2020a), which is modified after the approach reported in Inglis et al. (2018). Because 4 M HF could not re-dissolve the

250 samples completely, before loading on the first column, which is packed with 2 mL
251 anion exchange resin (Bio-Rad AG1-X8 200–400 mesh), the sample solutions with
252 precipitates were placed in an ultrasonic bath for 1 h, then centrifuged. The
253 supernatant was carefully taken up and loaded onto the column. Except for HFSE,
254 most matrix elements are removed with 32 mL (4 × 8 mL) of 4 M HF. During the
255 second stage, matrices were eluted with 12 mL of 12 M HNO_3 and 12 mL 3 M HNO_3
256 on the column with DGA resin. Finally, Zr was collected in 10 mL 3 M HNO_3 + 0.2
257 M HF. Recovery yields for Zr were higher than 90%. After evaporating to dryness, 16
258 M HNO_3 was added to the sample and then heated at 120 °C for 2 h to remove any
259 organic residues possibly coming from the resin. Then the samples were dried down
260 and dissolved in 0.5 M HNO_3 + 0.1 M HF in preparation for measurements on the
261 mass spectrometer.

262 Zirconium isotopic compositions were measured via the double spike method on
263 a *Thermo Fisher* Neptune Plus MC-ICP-MS at IPGP. Measurement details are
264 provided in Tian et al. (2020a, 2020b). Briefly, inert sample introduction kits,
265 including a Savillex™ PFA cyclonic spray chamber (CSC) and a Savillex™ sapphire
266 torch injector were used because the carrier acid has 0.1 M HF. $^{90}Zr^+$, $^{91}Zr^+$, $^{92}Zr^+$,
267 $^{94}Zr^+$, $^{95}Mo^+$ and $^{96}Zr^+$ were monitored simultaneously using Faraday cups with 10^{11}
268 Ω resistors. $^{91}Zr^+/^{90}Zr^+$, $^{94}Zr^+/^{90}Zr^+$ and $^{96}Zr^+/^{90}Zr^+$ were used for double spike data
269 processing, which was done by the *IsoSpike* add-on in the software package Iolite
270 (Creech and Paul, 2015). Before calculation, $^{95}Mo^+$ was used to correct interferences

from $^{94}Mo^{+}$ and $^{96}Mo^{+}$ on corresponding isobaric Zr ions. The data are reported against the IPGP-Zr standard; a calibration against other standards (e.g., zircon G1, NIST SRM 3169, 'NIST') can be found in Tian et al. (2020a). Total procedure blanks were <1 ng for Zr.

Results

The $\delta^{94/90}Zr_{IPGP\text{-}Zr}$ values we determined for BHVO-2 and GA are 0.048 ± 0.017‰ (2SD, n=4) and 0.13 ± 0.013‰ (2SD, n=7), respectively (Table S1), which agree well with data from the literature (Inglis et al., 2018; Tian et al., 2020a), confirming the accuracy of our data. Overall, the Zr isotope compositions of sedimentary rocks in this study are quite homogenous, ranging from 0.031 to 0.118‰ with an average $\delta^{94/90}Zr_{IPGP\text{-}Zr}$ of 0.078 ± 0.044‰ (2SD, n= 38), with a Zr-weighted average of 0.079 ± 0.044‰ (2SD, n=38). The $\delta^{94/90}Zr_{IPGP\text{-}Zr}$ values of Yimaguan, Luochuan, and Nileke loess range from 0.043 to 0.109‰, with an overall Zr-weighted average of 0.081 ± 0.044‰ (2SD, n = 12) and with individual weighted averages of 0.089 ± 0.028‰ (2SD, n = 6), 0.067± 0.043‰ (2SD, n = 3) and 0.082 ± 0.071‰ (2SD, n = 3), respectively. The three oceanic sediments from the DSDP sites outboard of the Lesser Antilles arc display a weighted average of $\delta^{94/90}Zr_{IPGP\text{-}Zr}$ of 0.073 ± 0.015‰ (2SD, n = 3). Glacial diamictites have similar Zr isotope compositions as those of the loess and oceanic sediments (Table S2 and S1). The $\delta^{94/90}Zr_{IPGP\text{-}Zr}$ values of 23 individual glacial diamictite composites vary from 0.031 to 0.118‰, with a Zr-weighted average of 0.078 ± 0.047‰ (2SD, n = 23). The Zr-weighted average

292 $\delta^{94/90}Zr_{IPGP\text{-}Zr}$ values of Mesoarchean, Paleoproterozoic, Neoproterozoic and Paleozoic
293 diamictite composites are 0.084 ± 0.033‰ (2SD, n = 4), 0.070 ± 0.052‰ (2SD, n =
294 6), 0.077 ± 0.055‰ (2SD, n = 10) and 0.090 ± 0.030‰ (2SD, n = 3), respectively.

295 **Discussion**

296 The different types of sedimentary samples analyzed here have relatively
297 homogenous Zr isotope compositions, reflecting limited Zr isotope fractionation
298 during the diverse geological processes by which these samples formed. Nevertheless,
299 we first consider the possible effects of mineral sorting and chemical weathering on
300 the Zr isotope compositions of these sedimentary samples, and then use the data to
301 calculate the average Zr isotope compositions of the UCC, BSE and bulk Earth.

302 1. **Zircon sorting has negligible effect on the Zr isotope compositions of**
303 **sedimentary samples**

304 On average, coarse-grained sedimentary samples show higher Zr and Hf
305 concentrations compared to fine-grained samples, which is usually interpreted to be
306 due to an enrichment of heavy minerals such as zircon and rutile via hydrodynamic
307 mineral sorting (Carpentier et al., 2009; Taylor and McLennan, 1985). Early studies
308 suggested that loess was enriched in Zr and Hf relative to the estimated average
309 composition of the UCC, reflecting concentration of zircon by aeolian processes
310 (Gallet et al., 1998; Taylor et al., 1983). Chauvel et al. (2014) argued that periglacial
311 loess samples had a large excess of Zr and Hf owing to the enrichment of zircons, but
312 that Chinese, Tajikistan, Argentinian and Sahara loess deposits do not show a zircon

313 excess effect, as evidenced by their $\Delta\varepsilon_{Hf}$ (Hf isotopic deviation from the terrestrial
314 array defined by Carpentier et al., 2009) and Nd/Hf ratio relationship, that is, low
315 Nd/Hf and negative $\Delta\varepsilon_{Hf}$ (Chauvel et al., 2014), even though most of these loess
316 samples have higher Zr/Al_2O_3 (12.3 ~ 26.0, data from Chauvel et al., 2014) ratios
317 compared to the UCC (12.5, Rudnick and Gao, 2014). It is worth noting that the
318 Western European loess samples studied in Chauvel et al. (2014), which showed a
319 zircon excess effect have some of the highest Zr/Al_2O_3 ratios: from 20.7 to 68.7.
320 Because zircons can have different Zr isotopic composition than their melts
321 (Chen et al., 2020; Guo et al., 2020; Inglis et al., 2019; Méheut et al., 2020; Tian et
322 al., 2020a; Zhang et al., 2019), zircon-enriched sedimentary samples may be
323 isotopically different. To quantify zircon enrichment, we first divided the oceanic
324 sediments and glacial diamictite composites into two groups according whether they
325 show higher Nd/Hf ratios relative to UCC . The samples whose Nd/Hf ratio is lower
326 than 5.1 are classified as having excess zircon. The Nd and Hf concentration of the
327 Chinese loess samples were not available, but considering that their Zr/Al_2O_3 ratios
328 (from 16.6 to 24.8) are comparable to those of Chinese loess samples in Chauvel et al.
329 (2014), and that the Yimaguan and Luochuan loess samples belong to the same loess
330 deposit as the one reported by Chauvel et al. (2014), these samples probably do not
331 record a zircon excess. The Xinjiang loess samples derive from a desert region, not
332 periglacial, so they are similar to other Chinese loess from Chinese Loess Plateau and
333 are also considered to not show a zircon excess effect. The two groups of samples

with or without zircon enrichment display average $\delta^{94/90}Zr_{IPGP\text{-}Zr}$ values of 0.075 ± 0.040‰ (2SD, n = 9) and 0.080 ± 0.046‰ (2SD, n = 29), respectively, which are statistically indistinguishable (t test, p value = 0.55). In addition, there is no correlation between $\delta^{94/90}Zr_{IPGP\text{-}Zr}$ values and Nd/Hf ratios (Fig. 2a, $R^2 = 0.01$), or Zr/Al_2O_3 ratios (Fig. 2b, $R^2 = 9.6\times10^{-7}$). The similarity of the Zr isotope composition between these two groups and the absence of correlation between $\delta^{94/90}Zr_{IPGP\text{-}Zr}$ Nd/Hf and Zr/Al_2O_3 illustrate that zircon addition or subtraction has not affected the Zr isotope composition of the sedimentary samples to a measurable extent.

2. **No measurable Zr isotope fractionation due to chemical weathering**

There has not yet been a study of Zr isotope behavior during chemical weathering. Nevertheless, the data for sedimentary samples reported here provide some insights. Terrigenous sedimentary rocks are the product of chemical weathering of preexisting rocks (Taylor and McLennan, 1985), and loess and most of the glacial diamictites studied here carry a chemical weathering signature (Gaschnig et al., 2014; Gaschnig et al., 2016; Sauzéat et al., 2015; Taylor et al., 1983).

As chemical weathering progresses, clay fractions increasingly dominate over primary minerals, and this is accompanied by a progressive increase of Al_2O_3 and $Fe_2O_{3\,(T)}$ but a decrease of SiO_2, Na_2O, K_2O, and CaO contents. Higher Al_2O_3/SiO_2, Fe_2O_3/SiO_2, CIA values and lower K_2O/Al_2O_3 values are common indicators of the degree of chemical weathering (Gallet et al., 1998; Gaschnig et al., 2014; Huang et al., 2020).

The Zr isotopic values of sedimentary samples analyzed in this study do not correlate with any of these weathering proxies (Fig. 3), suggesting that chemical weathering does not produce measurable Zr isotope fractionation. Additionally, the average $\delta^{94/90}Zr_{IPGP\text{-}Zr}$ values of glacial diamictite composites, loess and oceanic sediments plot within analytical error of each other, even though the oceanic sediments recorded more extensive chemical weathering, and fluid-rock exchange during transport and deposition compared to loess. Finally, there is no correlation between the $\delta^{7}Li$ and $\delta^{94/90}Zr_{IPGP\text{-}Zr}$ values of the glacial diamictite composites and oceanic sediments (Fig. 4), further indicating that chemical weathering has not affected Zr isotope compositions of these samples.

3. No evidence for Zr isotope fractionation of the UCC through space and time

The glacial diamictites studied here record evidence for a secular change in the composition of the UCC between the Archean and post-Archean, with Archean samples systematically enriched in platinum group elements (Chen et al., 2016), Cr, Ni, Co, (Gaschnig et al., 2016) and other transition metals such as Cu (Chen et al., 2019) relative to post-Archean diamictites.

These changes have been interpreted as reflecting a transition from a more mafic UCC to one similar to the present-day at the end of the Archean. A similar transition in UCC composition was earlier documented on the basis of the geochemistry of shales (Taylor and McLennan, 1983; Condie, 1993). However, this transition from

mafic to felsic UCC has been disputed, and a mostly felsic Hadean or early Archean crust has been proposed based on various geochemical lines of evidence, including the reinterpretation of the chemical composition of the terrigenous sediments (Greber and Dauphas, 2019; Ptáček et al., 2020), the Ti isotopic composition of shales (Greber et al., 2017) and Hf-O isotope compositions of the Hadean zircons (Harrison, 2009). Here, the Zr isotope composition of the diamictite composites show no secular trend (Fig. 5a), suggesting that the Zr isotopic composition of UCC has been constant since at least the Mesoarchean.

In addition, post-Archean diamictites, loess and oceanic sediments display indistinguishable Zr isotope compositions regardless of their geographic settings (Fig. 5b). Thus, it appears that the UCC is spatially homogenous when it comes to Zr isotopes.

4. Zr isotope composition of UCC and BSE

As demonstrated above, zircon enrichment or depletion, chemical weathering, and fluid-rock exchange processes, bulk UCC composition and geographic setting do not appear to have influenced the Zr isotopes of these sedimentary samples to any measurable extent. These samples can therefore be used to estimate the Zr isotope composition of the UCC.

Combining the data of sedimentary reference materials from the literature and Zr isotopic values of sedimentary samples reported in this study, we obtain a Zr-weighted UCC average $\delta^{94/90}Zr_{IPGP\text{-}Zr}$ of 0.077 ± 0.058‰ (2SD, n = 44) (Fig. 6a). This

value falls between the $\delta^{94/90}Zr_{IPGP\text{-}Zr}$ of the mantle (0.040 ± 0.044‰, n = 72), based on oceanic basalts (Inglis et al., 2019) and komatiites (Tian et al. 2020b), and evolved igneous rocks, which have higher $\delta^{94/90}Zr_{IPGP\text{-}Zr}$, showing a wide range from 0.053 to 0.475‰ based on the $\delta^{94/90}Zr_{IPGP\text{-}Zr}$ of granitoid reference materials (Fig. 6a and 6b, Table S3). The distinct and higher $\delta^{94/90}Zr_{IPGP\text{-}Zr}$ value of the UCC compared to the mantle (t test with a p value 2.88×10^{-10}, Fig. 6a) likely reflects a large-scale mixing of isotopically heavy felsic igneous rocks with isotopically light mantle-like mafic igneous rocks within the UCC.

The mass fractions of the main terrestrial reservoirs and their Zr abundances are presented in Table 1. Zirconium concentration is highest in the UCC (193ppm) (Rudnick and Gao, 2014), which is about two times that of the deep (middle and lower) crust (98 ppm) (Rudnick and Gao, 2014) and the oceanic sediments (82 ppm) (Jenner and O'Neill, 2012), and twenty times that of the mantle (9.8 ppm) (McDonough and Sun, 1995). However, the mantle still contains 92.38% of the Zr of the Earth, while the Zr fractions contributed by the UCC, deep continental crust and oceanic crust are only 3.34%, 3.02% and 1.26%, respectively. The Zr isotope composition of the deep continental crust is unknown. Considering its more mafic composition, it can be assumed that the lower continental crust has a similar Zr isotope composition to that of the mantle, as is the case for the oceanic crust. Therefore, the UCC is apparently the only isotopically fractionated reservoir within the BSE. Accordingly, the updated estimate of the BSE $\delta^{94/90}Zr_{IPGP\text{-}Zr}$ value is 0.041 ±

418 0.041‰ (Table 1). Given that the Earth's core does not likely contain any Zr (Li and
419 Fei, 2014), and that the Zr content of the hydrosphere is also negligible (1.84×10^{-7} %),
420 we infer that the bulk Earth has a $\delta^{94/90}Zr_{IPGP\text{-}Zr}$ of 0.041 ± 0.041‰.

421 **Conclusions**

422 Terrigenous and oceanic sedimentary samples that represent the UCC, with
423 depositional ages ranging from the Archean to the present have been analyzed in
424 order to estimate the Zr isotope composition of the UCC. Glacial diamictite
425 composites, loess and oceanic sediments display a restricted range of $\delta^{94/90}Zr_{IPGP\text{-}Zr}$,
426 which is systematically higher than $\delta^{94/90}Zr_{IPGP\text{-}Zr}$ of the mantle. The $\delta^{94/90}Zr_{IPGP\text{-}Zr}$ of
427 the sedimentary samples are constant regardless of their depositional ages, enrichment
428 or depletion of zircon, degree of chemical weathering and geographical locations,
429 reflecting a conservative Zr isotope composition of the UCC globally through time.
430 Combined with the $\delta^{94/90}Zr_{IPGP\text{-}Zr}$ values of sedimentary reference materials reported
431 in the literature, we derive a $\delta^{94/90}Zr_{IPGP\text{-}Zr}$ of the UCC of 0.077± 0.058‰ (2SD, n =
432 44).

433

434

435

Acknowledgements

We thank the two anonymous reviewers for their thorough reviews that greatly improved the quality of this paper and the Editor for the efficient handling of our manuscript.

SYT greatly appreciates a fellowship from the China Scholarship Council. Pascale Louvat, Barthélémy Julien and Pierre Burckel are thanked for technical support of the (MC-)ICP-MS at IPGP. Nan Xiaoyuan and Gong Yingzeng are thanked for the collection of major and trace element data for loess. This work was supported by the ERC under the European Community's H2020 framework program/ERC grant agreement No. 637503 (Pristine) awarded to FM. Additional support from the UnivEarthS Labex program (numbers: ANR-10-LABX-0023 and ANR-11-IDEX-0005-02). Parts of this work were supported by IPGP multidisciplinary program PARI, and by Region île-de-France SESAME Grant (no. 12015908). Collection and investigations of the glacial diamictites was supported by NSF grant EAR-1321954 and a grant from the State Key Laboratory of Geological Processes and Mineral Resources at China University of Geosciences in Wuhan.

Figures

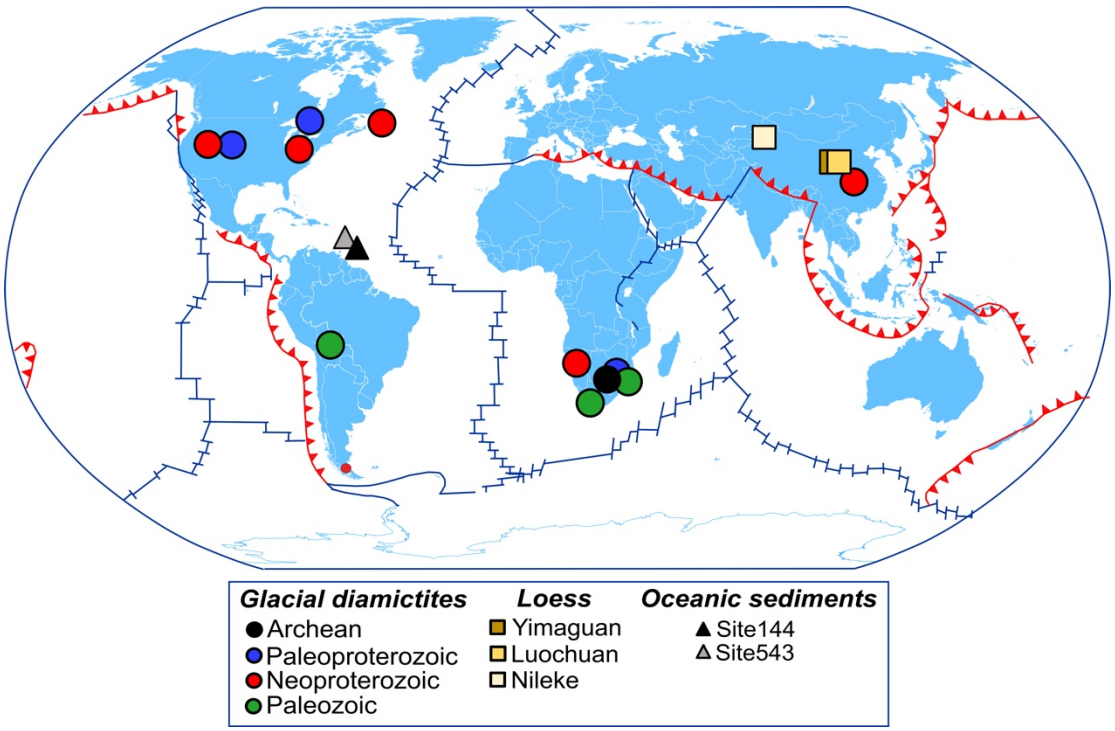

Fig. 1. Sample locality map, modified after Gaschnig et al. (2014) and Huang et al. (2016).

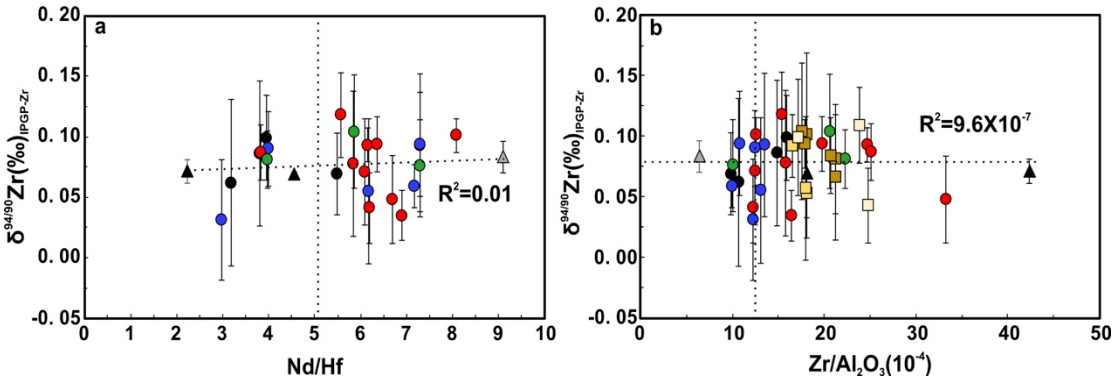

Fig. 2. $\delta^{94/90}Zr_{IPGP-Zr}$ vs. (a) Nd/Hf for oceanic sediments and glacial diamictite composites (b) Zr/Al_2O_3 for loess, oceanic sediments and glacial diamictite composites, with symbols as in Fig. 1. There is no correlation between $\delta^{94/90}Zr_{IPGP-Zr}$ and Nd/Hf (R^2=0.01), or Zr/Al_2O_3 values (R^2=9.6×10^{-7}). The Nd, Hf, Zr and Al_2O_3 data are from: Gaschnig et al. (2016) for glacial diamictite composites, Hao et al. (2012) and Tsai et al. (2014) for loess, and Carpentier et al. (2008 and 2009) for oceanic sediments. The loess samples are not included in (a) because their Nd and Hf data are not available from the literature. The vertical lines represent UCC ratios, data from Rudnick and Gao et al. (2014).

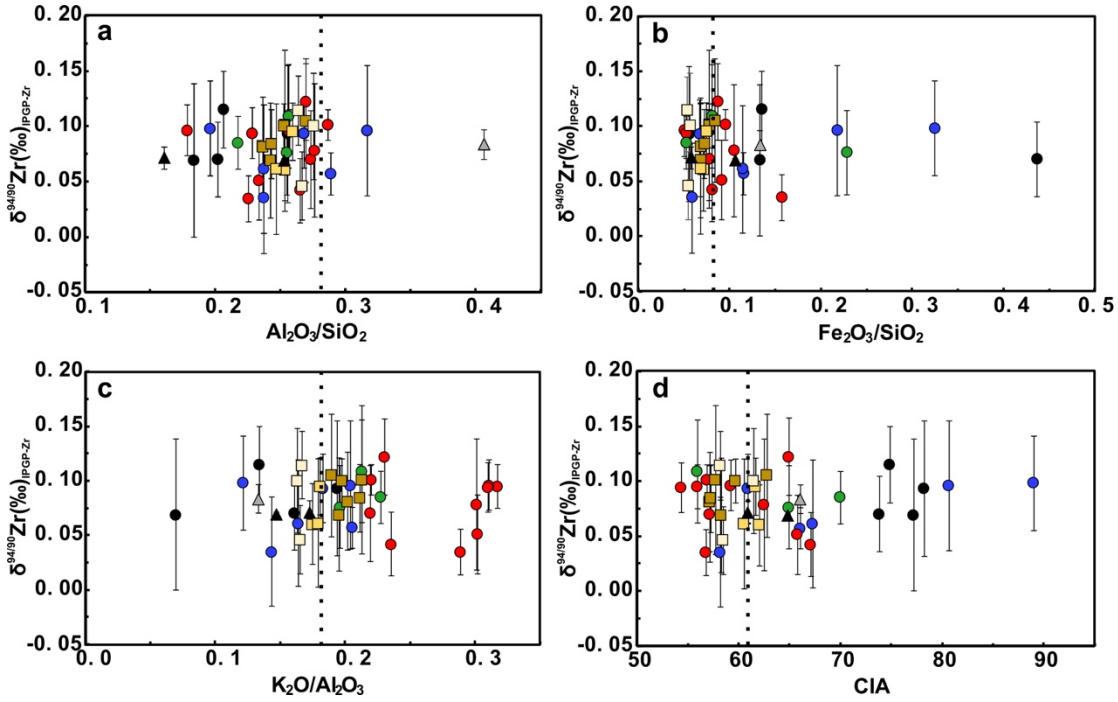

480

481 Fig. 3. $\delta^{94/90}Zr_{IPGP-Zr}$ vs. (a) Al_2O_3/SiO_2 (b) Fe_2O_3/SiO_2 (c) K_2O_3/Al_2O_3 and (d)

482 CIA values for all the samples in this study, with symbols as in Fig. 1. The elemental

483 data sources are the same as listed in Fig. 2. The vertical lines represent UCC ratios,

484 data from Rudnick and Gao et al. (2014) and Sauzéat et al. (2015.

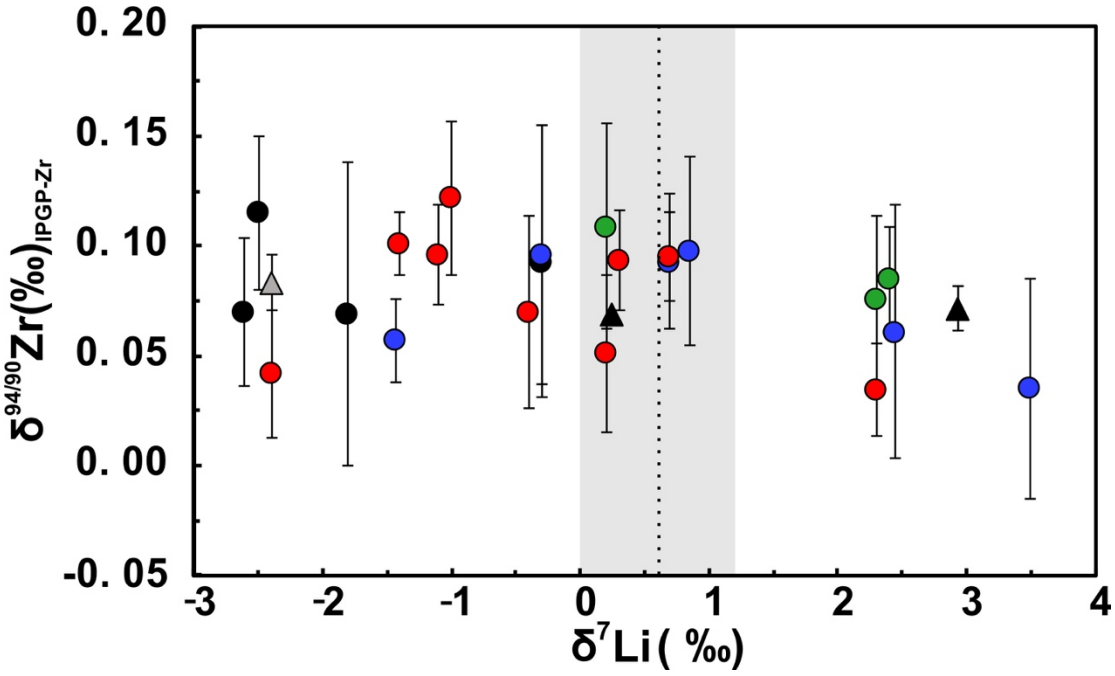

485

486 Fig. 4. $\delta^{94/90}Zr_{IPGP\text{-}Zr}$ vs $\delta^{7}Li$ in glacial diamictite composites and oceanic

487 sediments, with symbols as in Fig. 1. The $\delta^{7}Li$ data are from Li et al. (2016) and Tang

488 et al. (2014). The vertical line and grey band denote the $\delta^{7}Li$ suggested by Sauzéat et

489 al. (2015) for average UCC.

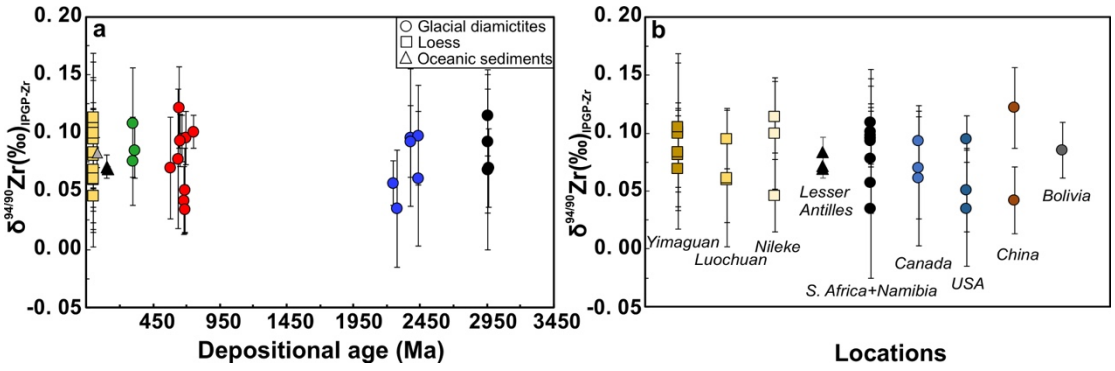

Fig. 5. (a) Depositional age vs. $\delta^{94/90}Zr_{IPGP\text{-}Zr}$ for loess, oceanic sediments and glacial diamictite composites (b) $\delta^{94/90}Zr_{IPGP\text{-}Zr}$ of loess, oceanic sediments and post-Archean glacial diamictite composites from different locations. The depositional ages of oceanic sediments and glacial diamictite composites are from Carpentier et al. (2008) and Greaney et al. (2020), respectively. The depositional ages of loess vary from 0.56 kyr to 1.24 kyr (Hao et al., 2012), but the individual age for each loess sample is unknown. In this figure, their ages are set at 0.001Ma.

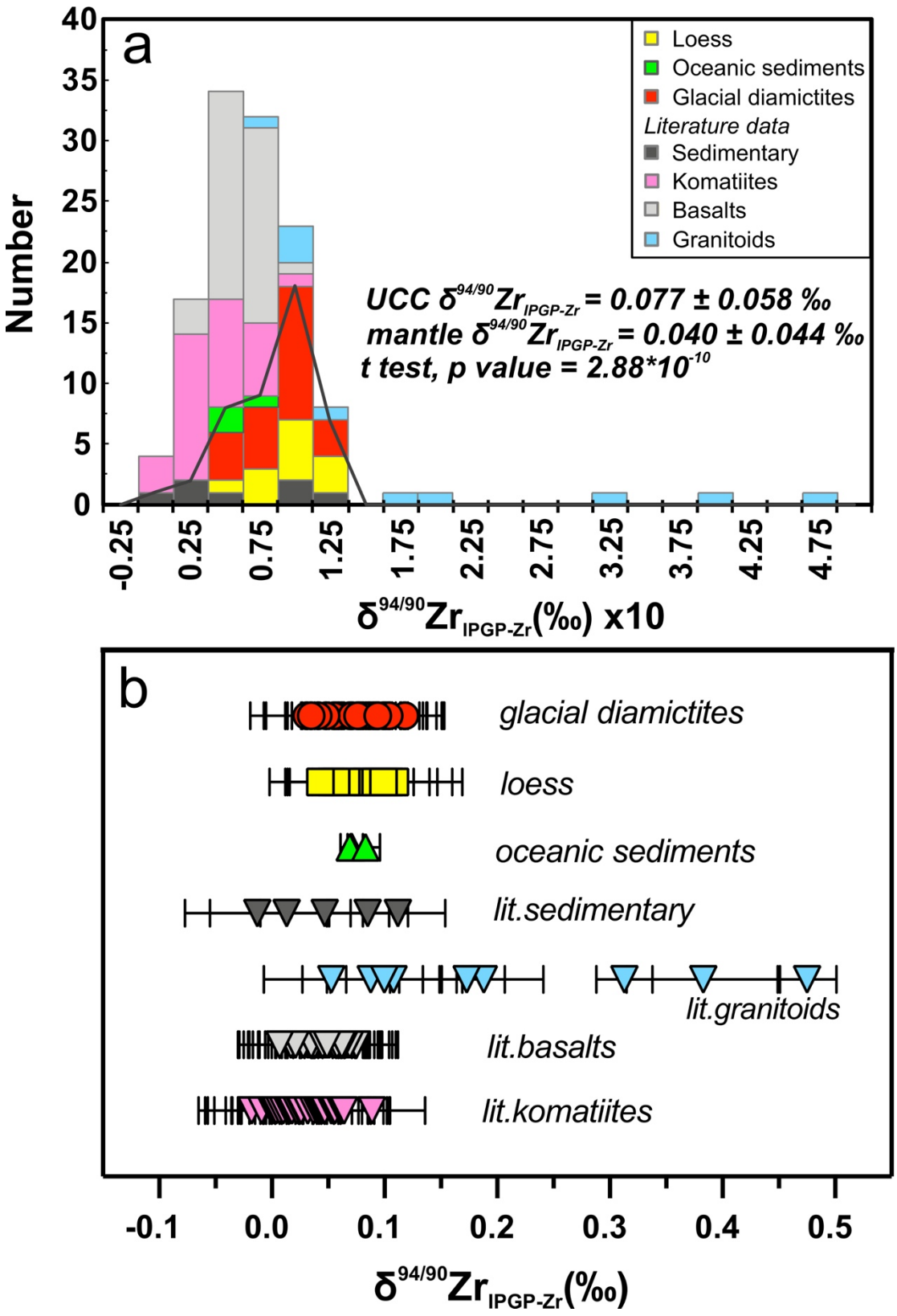

Fig. 6. (a) Histogram of the distribution frequency of $\delta^{94/90}Zr_{IPGP-Zr}$ and (b) the diagram of Zr isotope compositions of samples from this study and literature data for

clastic sedimentary rocks (Feng et al., 2020; Tian et al., 2020a), granitoid rocks (Feng et al., 2020; Inglis et al., 2018; Tian et al., 2020a), komatiites (Tian et al., 2020b) and oceanic basalts (Inglis et al., 2019). The black curve denotes the distribution of $\delta^{94/90}Zr_{IPGP\text{-}Zr}$ values of all the sedimentary samples.

524 **Table**

525 Table 1. Mass balance model for Zr isotope compositions of BSE

Reservoirs	**Mass(10^{21}kg)[a]**	**Mass(%)**	**Zr(ppm)[b]**	**Zr(%)**	**$\delta^{94/90}Zr_{IPGP\text{-}Zr}$ (‰)**
Hydrosphere	2	0.05	3.90×10^{-5}	1.82×10^{-7}	? [c]
Upper continental crust	7.4	0.18	193	3.34	0.077 ± 0.058
Deep continental crust (LCC + MCC)	13.2	0.33	98	3.02	0.040 ± 0.044
Oceanic crust	6.6	0.16	82	1.26	0.040 ± 0.044
Mantle	4008	99.28	9.8	92.38	0.040 ± 0.044
Bulk Silicate Earth	4037.2	100	10.5	100	0.041 ± 0.041[d]

526 [a] The mass data of reservoirs are from Huang et al. (2020).

527 [b] Zirconium content of hydrosphere is from Gaillardet et al. (2003). Zirconium

528 concentration data of upper and deep continental crust, oceanic crust and Bull Silicate

529 Earth are from Rudnick and Gao (2014), Jenner and O'Neill (2012) and McDonough

530 and Sun (1995).

531 [c] $\delta^{94/90}Zr_{IPGP\text{-}Zr}$ of hydrosphere has not been studied yet.

532 [d] The error means 2SD, calculated via error propagation.

References

Brown, M., Johnson, T., Gardiner, N.J., 2020. Plate Tectonics and the Archean Earth. Annu. Rev. Earth Planet. Sci. 48, 291-320.

Carpentier, M., Chauvel, C., Mattielli, N., 2008. Pb–Nd isotopic constraints on sedimentary input into the Lesser Antilles arc system. Earth Planet. Sci. Lett 272, 199-211.

Carpentier, M., Chauvel, C., Maury, R.C., Mattielli, N., 2009. The "zircon effect" as recorded by the chemical and Hf isotopic compositions of Lesser Antilles forearc sediments. Earth Planet. Sci. Lett 287, 86-99.

Chauvel, C., Garçon, M., Bureau, S., Besnault, A., Jahn, B.-m., Ding, Z., 2014. Constraints from loess on the Hf–Nd isotopic composition of the upper continental crust. Earth Planet. Sci. Lett 388, 48-58.

Chen, K., Rudnick, R.L., Wang, Z., Tang, M., Gaschnig, R.M., Zou, Z., He, T., Hu, Z., Liu, Y., 2019. How mafic was the Archean upper continental crust? Insights from Cu and Ag in ancient glacial diamictites. Geochim. Cosmochim. Acta.

Chen, K., Walker, R.J., Rudnick, R.L., Gao, S., Gaschnig, R.M., Puchtel, I.S., Tang, M., Hu, Z.C., 2016. Platinum-group element abundances and Re–Os isotopic systematics of the upper continental crust through time: Evidence from glacial diamictites. Geochim. Cosmochim. Acta 191, 1-16.

Chen, X., Wang, W., Zhang, Z., Nie, N.X., Dauphas, N., 2020. Evidence from Ab Initio and Transport Modeling for Diffusion-Driven Zirconium Isotopic Fractionation in Igneous Rocks. ACS Earth Space Chem. 4, 1572-1595.

Condie, K.C., 1993. Chemical composition and evolution of the upper continental crust: contrasting results from surface samples and shales. Chem. Geol. 104, 1-37.

Condie, K.C., 2005. High field strength element ratios in Archean basalts: a window to evolving sources of mantle plumes? Lithos 79, 491-504.

Deng, Z., Chaussidon, M., Savage, P., Robert, F., Pik, R., Moynier, F., 2019. Titanium isotopes as a tracer for the plume or island arc affinity of felsic rocks. Proc. Natl. Acad. Sci. U.S.A. 116, 1132-1135.

Dhuime, B., Hawkesworth, C.J., Cawood, P.A., Storey, C.D., 2012. A change in the geodynamics of continental growth 3 billion years ago. Science 335, 1334-1336.

Feng, L., Hu, W., Jiao, Y., Zhou, L., Zhang, W., Hu, Z., Liu, Y., 2020. High-precision stable zirconium isotope ratio measurements by double spike thermal ionization mass spectrometry. J. Anal. At. Spectrom. 35, 736-745.

Gaillardet, J., Viers, J., Dupré, B., 2014. Trace elements in river waters, Treatise on Geochemistry, 2nd ed. Elsevier, Hoboken, N. J., pp. 195–235.

Gallet, S., Jahn, B.-m.J., Van Vliet-Lanoë, B., Dia, A., Rossello, E., 1998. Loess geochemistry and its application for particle origin and composition of the upper continental crust. Earth Planet. Sci. Lett 156, 157-172.

Gaschnig, R.M., Reinhard, C.T., Planavsky, N.J., Wang, X., Asael, D., Chauvel, C., 2017. The Molybdenum Isotope System as a Tracer of Slab Input in Subduction

Zones: An Example From Martinique, Lesser Antilles Arc. Geochemistry, Geophysics, Geosystems 18, 4674-4689.
Gaschnig, R.M., Rudnick, R.L., McDonough, W.F., Kaufman, A.J., Hu, Z.C., Gao, S., 2014. Onset of oxidative weathering of continents recorded in the geochemistry of ancient glacial diamictites. Earth Planet. Sci. Lett 408, 87-99.
Gaschnig, R.M., Rudnick, R.L., McDonough, W.F., Kaufman, A.J., Valley, J.W., Hu, Z., Gao, S., Beck, M.L., 2016. Compositional evolution of the upper continental crust through time, as constrained by ancient glacial diamictites. Geochim. Cosmochim. Acta 186, 316-343.
Goldschmidt, V., 1933. Grundlagen der quantitativen Geochemie. Fortschr. Mienral. Kirst. Petrogr 17, 112.
Gong, Y.Z., Xia, Y., Huang, F., Yu, H.M., 2017. Average iron isotopic compositions of the upper continental crust: constrained by loess from the Chinese Loess Plateau. Acta Geochimica 36, 125-131.
Greaney, A.T., Rudnick, R.L., Romaniello, S.J., Johnson, A.C., Gaschnig, R.M., Anbar, A.D., 2020. Molybdenum isotope fractionation in glacial diamictites tracks the onset of oxidative weathering of the continental crust. Earth Planet. Sci. Lett 534.
Greber, N.D., Dauphas, N., 2019. The chemistry of fine-grained terrigenous sediments reveals a chemically evolved Paleoarchean emerged crust. Geochim. Cosmochim. Acta 255, 247-264.
Greber, N.D., Dauphas, N., Bekker, A., Ptáček, M.P., Bindeman, I.N., Hofmann, A., 2017. Titanium isotopic evidence for felsic crust and plate tectonics 3.5 billion years ago. Science 357, 1271-1274.
Guo, J.L., Wang, Z., Zhang, W., Moynier, F., Cui, D., Hu, Z., Ducea, M.N., 2020. Significant Zr isotope variations in single zircon grains recording magma evolution history. Proc. Natl. Acad. Sci. U. S. A. 117, 21125-21131.
Hao, Q.Z., Wang, L., Oldfield, F., Peng, S.Z., Qin, L., Song, Y., Xu, B., Qiao, Y.S., Bloemendal, J., Guo, Z.T., 2012. Delayed build-up of Arctic ice sheets during 400,000-year minima in insolation variability. Nature 490, 393.
Harrison, T.M., 2009. The Hadean Crust: Evidence from >4 Ga Zircons. Annu. Rev. Earth Planet. Sci. 37, 479-505.
Harrison, T.M., Blichert-Toft, J., Müller, W., Albarede, F., Holden, P., Mojzsis, S.J., 2005. Heterogeneous Hadean Hafnium: Evidence of Continental Crust at 4.4 to 4.5 Ga. Science 310, 1947-1950.
Hoare, L., Klaver, M., Saji, N.S., Gillies, J., Parkinson, I.J., Lissenberg, C.J., Millet, M.-A., 2020. Melt chemistry and redox conditions control titanium isotope fractionation during magmatic differentiation. Geochim. Cosmochim. Acta 282, 38-54.
Huang, F., Xu, J., Zhang, J., 2016. U-series disequilibria in subduction zone lavas: Inherited from subducted slabs or produced by mantle in-growth melting? Chem. Geol. 440, 179-190.

615 Huang, T.Y., Teng, F.Z., Rudnick, R.L., Chen, X.Y., Hu, Y., Liu, Y.S., Wu, F.Y.,
616 2020. Heterogeneous potassium isotopic composition of the upper continental crust.
617 Geochim. Cosmochim. Acta 278, 122-136.
618 Ibañez-Mejia, M., Tissot, F.L., 2019. Extreme Zr stable isotope fractionation during
619 magmatic fractional crystallization. Sci. Adv. 5, eaax8648.
620 Inglis, E.C., Creech, J.B., Deng, Z.B., Moynier, F., 2018. High-precision zirconium
621 stable isotope measurements of geological reference materials as measured by double-
622 spike MC-ICPMS. Chem. Geol. 493, 544-552.
623 Inglis, E.C., Moynier, F., Creech, J., Deng, Z.B., Day, J.M.D., Teng, F.-Z., Bizzarro,
624 M., Jackson, M., Savage, P., 2019. Isotopic fractionation of zirconium during
625 magmatic differentiation and the stable isotope composition of the silicate Earth.
626 Geochim. Cosmochim. Acta 250, 311-323.
627 Jenner, F.E., O'Neill, H.S.C., 2012. Analysis of 60 elements in 616 ocean floor
628 basaltic glasses. Geochem. Geophys. Geosyst. 13, 1-11.
629 Johnson, B.W., Goldblatt, C., 2017. A secular increase in continental crust nitrogen
630 during the Precambrian. Geochem. Perspect. Lett. 4, 24-28.
631 Korenaga, J., 2013. Initiation and Evolution of Plate Tectonics on Earth: Theories and
632 Observations. Annu. Rev. Earth Planet. Sci. 41, 117-151.
633 Li, J., Fei, Y., 2014. Experimental Constraints on Core Composition, Treatise on
634 Geochemistry, 2nd ed. Elsevier, Hoboken, N. J., pp. 527–553.
635 Li, S., Gaschnig, R.M., Rudnick, R.L., 2016. Insights into chemical weathering of the
636 upper continental crust from the geochemistry of ancient glacial diamictites.
637 Geochim. Cosmochim. Acta 176, 96-117.
638 Lodders, K., 2003. Solar system abundances and condensation temperatures of the
639 elements. Astrophys. J. 591, 1220.
640 McDonough, W.F., Sun, S.-S., 1995. The composition of the Earth. Chem. Geol. 120,
641 223-253.
642 Méheut, M., Ibañez-Mejia, M., Tissot, F.L., 2020. Drivers of zirconium isotope
643 fractionation in Zr-bearing phases and melts: The roles of vibrational, nuclear field
644 shift and diffusive effects. Geochim. Cosmochim. Acta 292, 217-234.
645 Mundl, A., Walker, R.J., Reimink, J.R., Rudnick, R.L., Gaschnig, R.M., 2018.
646 Tungsten-182 in the upper continental crust: Evidence from glacial diamictites.
647 Chem. Geol. 494, 144-152.
648 Nan, X.Y., Yu, H.M., Rudnick, R.L., Gaschnig, R.M., Xu, J., Li, W.Y., Zhang, Q.,
649 Jin, Z.D., Li, X.H., Huang, F., 2018. Barium isotopic composition of the upper
650 continental crust. Geochim. Cosmochim. Acta 233, 33-49.
651 Nesbitt, H., Young, G., 1982. Early Proterozoic climates and plate motions inferred
652 from major element chemistry of lutites. nature 299, 715-717.
653 Niu, Y.L., 2004. Bulk-rock Major and Trace Element Compositions of Abyssal
654 Peridotites: Implications for Mantle Melting, Melt Extraction and Post-melting
655 Processes Beneath Mid-Ocean Ridges. J Petrol 45, 2423-2458.

Plank, T., Langmuir, C.H., 1998. The chemical composition of subducting sediment and its consequences for the crust and mantle. Chem. Geol. 145, 325-394.
Ptáček, M.P., Dauphas, N., Greber, N.D., 2020. Chemical evolution of the continental crust from a data-driven inversion of terrigenous sediment compositions. Earth Planet. Sci. Lett 539, 116090.
Rudnick, R.L., Gao, S., 2014. Composition of the Continental Crust, Treatise on Geochemistry, 2nd ed. Elsevier, Hoboken, N. J., pp. 1-51.
Sauzéat, L., Rudnick, R.L., Chauvel, C., Garçon, M., Tang, M., 2015. New perspectives on the Li isotopic composition of the upper continental crust and its weathering signature. Earth Planet. Sci. Lett 428, 181-192.
Tang, M., Chen, K., Rudnick, R.L., 2016. Archean upper crust transition from mafic to felsic marks the onset of plate tectonics. Science 351, 372-375.
Tang, M., Rudnick, R.L., Chauvel, C., 2014. Sedimentary input to the source of Lesser Antilles lavas: A Li perspective. Geochim. Cosmochim. Acta 144, 43-58.
Taylor, S., McLennan, S., McCulloch, M., 1983. Geochemistry of loess, continental crustal composition and crustal model ages. Geochim. Cosmochim. Acta 47, 1897-1905.
Taylor, S.R., McLennan, S.M., 1985. The Continental Crust: its composition and evolution. Blackwell Scientific Publications.
Tian, S.Y., Inglis, E.C., Creech, J.B., Zhang, W., Wang, Z.C., Hu, Z.C., Liu, Y.S., Moynier, F., 2020a. The zirconium stable isotope compositions of 22 geological reference materials, 4 zircons and 3 standard solutions. Chem. Geol. 555, 119791.
Tian, S.Y., Moynier, F., Inglis, E.C., Creech, J., Bizzarro, M., Siebert, J., Day, J.M.D., Puchtel, I.S., 2020b. Zirconium isotopic composition of the mantle through time. Geochem. Perspect. Lett. 15, 40-43.
Tsai, P.H., You, C.F., Huang, K.F., Chung, C.H., Sun, Y.B., 2014. Lithium distribution and isotopic fractionation during chemical weathering and soil formation in a loess profile. J. Asian Earth Sci. 87, 1-10.
Valley, J., Lackey, J., Cavosie, A., Clechenko, C., Spicuzza, M., Basei, M., Bindeman, I., Ferreira, V., Sial, A., King, E., 2005. 4.4 billion years of crustal maturation: oxygen isotope ratios of magmatic zircon. Contrib. to Mineral. Petrol. 150, 561-580.
Wang, S.J., Rudnick, R.L., Gaschnig, R.M., Wang, H., Wasylenki, L.E., 2019. Methanogenesis sustained by sulfide weathering during the Great Oxidation Event. Nat. Geosci. 12, 296-300.
Wilde, S.A., Valley, J.W., Peck, W.H., Graham, C.M., 2001. Evidence from detrital zircons for the existence of continental crust and oceans on the Earth 4.4 Gyr ago. Nature 409, 175-178.
Zhang, W., Wang, Z., Moynier, F., Inglis, E., Tian, S., Li, M., Liu, Y., Hu, Z., 2019. Determination of Zr isotopic ratios in zircons using laser-ablation multiple-collector inductively coupled-plasma mass-spectrometry. J. Anal. At. Spectrom. 34, 1800-1809.

698